Maximum Vortex-Induced Side Force

J. Peter Reding* and Lars E. Ericsson†
Lockheed Missiles & Space Co., Inc., Sunnyvale, Calif.

A method of determining the maximum vortex-induced side force on slender bodies at high angle of attack and zero sideslip is presented. The maximum stationary vortex asymmetry is related to the maximum instantaneous asymmetry for nonstationary separation on a cylinder normal to the flow. Thus, the two-dimensional peak nonsteady lift to steady drag ratio for a cylinder is indicative of the maximum possible stationary side-force to normal-force ratio on a slender body. An effective crossflow Reynolds number is used to relate three-dimensional Reynolds number effects to two-dimensional cylinder results. Similar techniques are used to predict the maximum additional lift generated by asymmetric vortex shedding.

Nomenclature

c = reference length = d_{max}
d = body diameter
d^* = equivalent diameter, defined by Eq. (1)
D_{2D} = cross-sectional drag; coefficient $c_D = \dfrac{D_{2D}}{(\rho V^2/2)d}$
M = freestream Mach number
l = body length
l_N = length of nose tip
L_{2D} = cross-sectional lift; coefficient $c_l = \dfrac{L_{2D}}{(\rho V^2/2)d}$
N = normal force; coefficient $C_N = \dfrac{N}{(\rho V^2/2)S}$
r_B = base radius
r_N = nose-tip radius
Re_d = Reynolds number based on d and freestream conditions
$(Re)_{eff}$ = effective Reynolds number, Eq. (3)
S = reference area = $\pi c^2/4$
V = freestream velocity
x = axial coordinate, distance from body apex
Y = side force; coefficient $C_Y = \dfrac{Y}{(\rho V^2/2)S}$
α = angle of attack
β = angle of sideslip
θ_c = cone half-angle
θ_N = nose semivertex angle ($\theta_N = \theta_c$ for conic tip)
ρ = air density
σ = surface flow inclination (Fig. 7)
ϕ = azimuth, or roll angle

Subscripts

AV = asymmetric vortex shedding
B = base
N = nose
peak = peak-to-peak amplitude
s = separation
SV = symmetric vortex shedding
UV = unsteady vortex shedding

Superscripts

$([\,]^2)^{1/2}$ = root-mean-square value
$[\,]$ = parameter value at the aerodynamic center

Presented as Paper 77-1155 at the AIAA 4th Atmospheric Flight Mechanics Conference, Hollywood, Fla., Aug. 8-10, 1977; submitted Sept. 20, 1977; revision received March 20, 1978.

Index categories: LV/M Aerodynamics; Subsonic Flow; Jets, Wakes, and Viscid-Inviscid Flow Interactions.

*Research Specialist. Member AIAA.
†Consulting Engineer. Associate Fellow AIAA.

Introduction

HIGH-ANGLE-OF-ATTACK requirements for both missiles and aircraft have precipitated renewed interest in the vortex-induced side forces that occurs at zero sideslip on slender bodies.[1-21] At high angles of attack, the flow separating off the leeside of a slender body rolls up into a pair of symmetric vortices. Above some critical high angle of attack, the vortices become asymmetric, generating significant side forces that can cause an aircraft to spin or a missile to tumble if these vortex effects have not been considered in the control system design.

Measurements on ogives, cones, and paraboloids have shown that the vortex-induced side force can be considerably larger than the normal force (Fig. 1).[4] Although small nose bluntness initially has an alleviating effect, substantial side forces have been measured for moderate to large nose bluntness (Fig. 2).[5,6,9] The vortex-induced side force becomes negligible at high supersonic speeds (when the crossflow approaches sonic speed). However, it is of concern for high-performance aircraft and missiles operating at high angles of attack in the subsonic and transonic speed regimes. Consequently, an extensive effort has been expended to generate a data base from which to predict the vortex-induced side forces for full-scale flight vehicles. The approach has been to construct a mathematical model where the steady three-dimensional vortex array is related to the nonsteady two-dimensional vortex street using the principle of space-time equivalence. Such techniques rely on empirically determined constants for the vortex strength and can reliably predict only the experimental results from which the constants are determined. The problem is that a single set of experimental

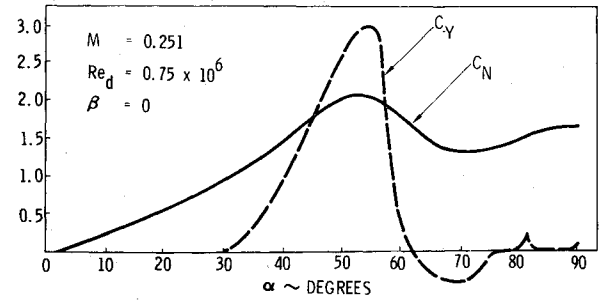

Fig. 1 Normal- and side-force coefficients for a 3.5 l/d tangent ogive.[4]

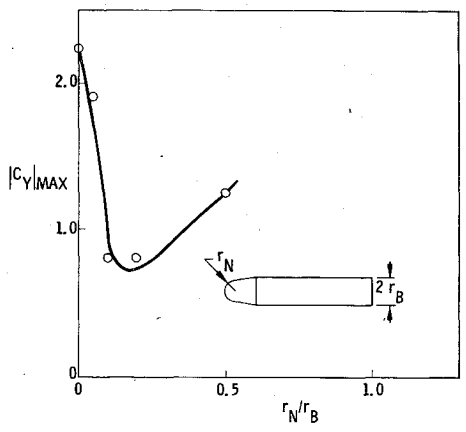

Fig. 2 Effect of nose bluntness on maximum vortex-induced side force.[5]

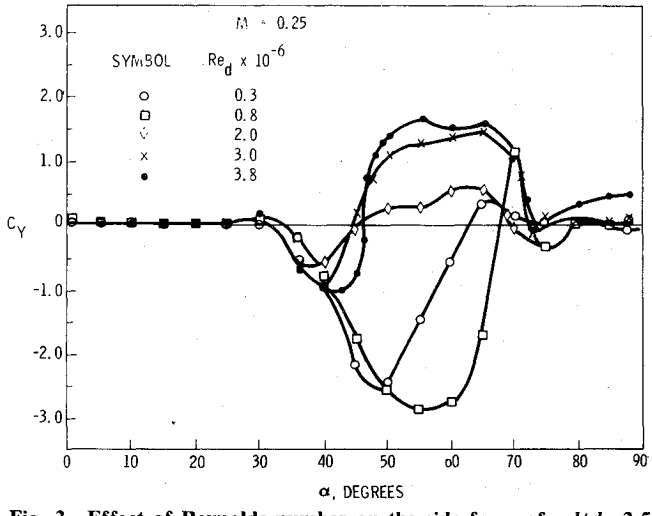

Fig. 3 Effect of Reynolds number on the side force of a $l/d=3.5$ ogive.[20]

data is but one of many alternative results possible for the same configuration, since the side force is extremely sensitive to Reynolds number, roll angle, surface roughness, Mach number, etc. The present approach is to establish bounds for the maximum possible vortex-induced side force and thus furnish the information needed for control system design.

Discussion

Reynolds number exercises a dominating influence on the side-force characteristics (Fig. 3).[4,6-8,11,20] More surprising is the extreme sensitivity to minute model asymmetries illustrated by the dramatic effect of roll orientation (Fig. 4a). Minute asymmetries of the presumably symmetric nose tips are the culprits (compare Figs. 4a and 4b).‡ This is demonstrated further by the equally dramatic effect of surface finish on side-force characteristics (Fig. 4c). A correlation of the peak side-force coefficients of Fig. 4b indicates that the side force is bounded by some maximum possible value and that the roll orientation only causes the side force to shift between these positive and negative limits.

The foregoing illustrates the problem encountered with the standard approach. A theory based on a limited set of experimental data, or even upon an average of a large sample of data, cannot be expected to be a generally applicable tool unless it accounts for all possible sensitivities, known and unknown. To determine the maximum possible side force

‡Reference 9 indicates that a 0.05-deg nose misalignment is sufficient to alter the vortex patterns.

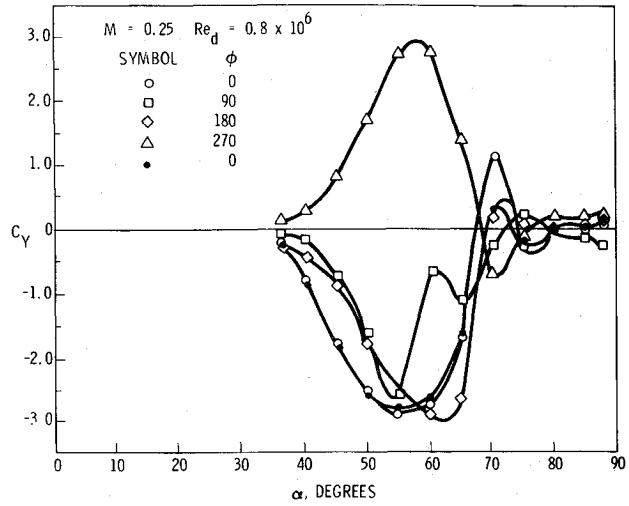

a) Effect of body roll angle

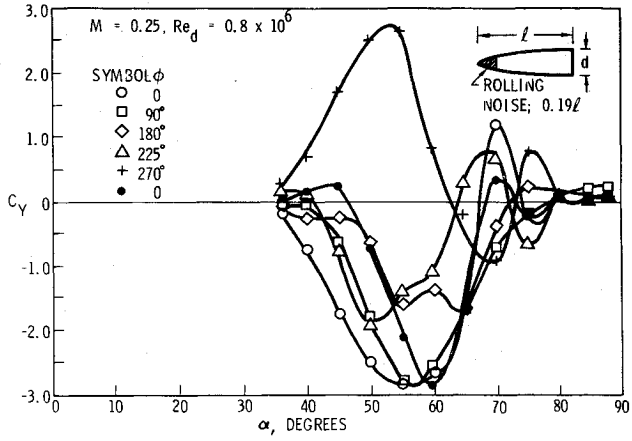

b) Effect of nose roll angle

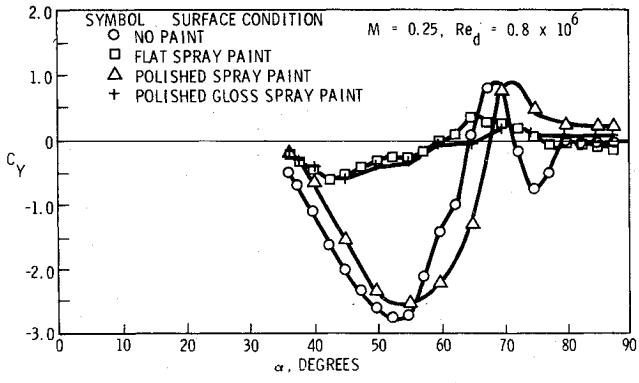

c) Effect of surface finish

Fig. 4 Effect of minute geometric asymmetries on the side force of a $l/d=3.5$ ogive.[20]

experimentally is also very difficult. In order to make sure that the maximum side force has been measured in a wind-tunnel test, the model has to be tested through the complete 360 deg of roll with full-scale manufacturing misalignments, surface irregularities, Mach number, and Reynolds number simulated on the subscale model. Even if such total simulation were possible, the results from such extensive, time-consuming, and expensive wind-tunnel tests could be invalidated by subsequent minor configuration changes. In flight, the control system must be capable of coping with the maximum possible vortex-induced side force, since a particular missile maneuver could "lock in" the particular vortex asymmetry that gives maximum side force. The present

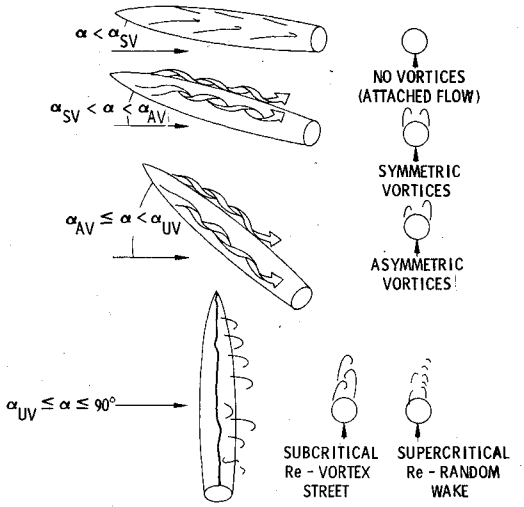

Fig. 5 Effect of angle of attack on the leeside flowfield.

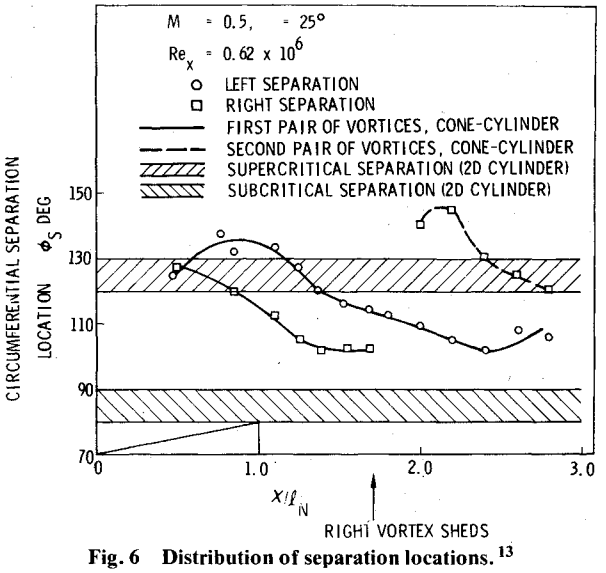

Fig. 6 Distribution of separation locations.[13]

analysis develops the means for predicting the maximum possible vortex-induced side force.

If the control system is unable to cope with this maximum possible side force, as is the case for the aircraft spin-stall problem where the control surfaces are stalled, steps can be taken to limit the side force. For vehicles that fly coordinated maneuvers (i.e., maintain a fixed roll orientation), such as aircraft and bank-to-turn missiles, small nose strakes provide an effective fix. They have been shown to reduce and even eliminate the vortex-induced side forces on noses[4,6,11,20] and complete aircraft configurations.[3,17] It is important that the strakes be located very near the nose tip. Full-length strakes and aft strakes (that simulate the conduit fairings on some missiles) have been shown to increase the vortex-induced side force.[14]

Strakes cannot be used for configurations that are allowed to roll. Conceivably, strakes could worsen the vortex-induced side-force problem for certain roll orientations. As has already been discussed, moderate nose bluntness can reduce the vortex-induced side force (Fig. 2).[5] Also, a circumferential boundary-layer trip, such as a nose ring[14] or a band of vortex generators,[9] has been shown to be moderately effective in reducing the vortex-induced side force.

All of these fixes are sensitive to Reynolds number, Mach number, etc., and are very dependent on vehicle geometry and flight profile. Thus, they must be developed experimentally for each individual case, although the literature is replete with

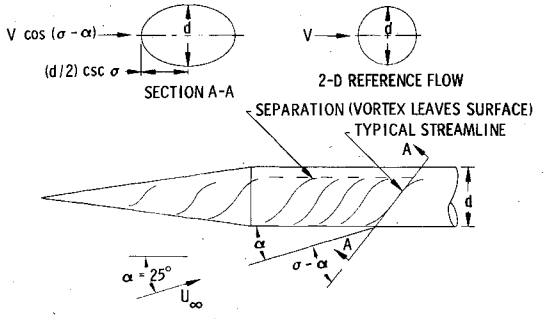

Fig. 7 Typical streamline trajectories.[13]

examples (such as those just cited) that can be used as a starting point for development.

Maximum Vortex-Induced Side Force

As a slender body is pitched through the angle-of-attack range $0 \leq \alpha \leq 90$ deg, it experiences four distinct flow patterns that reflect the diminishing influence of the axial flow component (Fig. 5). At low angles of attack ($0 \leq \alpha < \alpha_{SV}$), the axial flow dominates and the flow is attached. At intermediate angles of attack ($\alpha_{SV} \leq \alpha < \alpha_{AV}$), crossflow sweeps the boundary layer to the leeward side, where it separates and rolls up into a symmetric vortex pair. At high angles of attack ($\alpha_{AV} \leq \alpha < \alpha_{UV}$), crossflow effects start to dominate and the vortices become asymmetric, thereby producing a side force for zero sideslip. Finally, at very high angles of attack ($\alpha \geq \alpha_{UV}$), the crossflow dominates completely and the boundary layer is shed in the form of a Karman vortex street or a random wake, depending upon whether the Reynolds number is subcritical or supercritical. On pointed slender cones, development of symmetric vortices has been observed when the angle of attack exceeds the cone half-angle, both for laminar and turbulent flow and at all speeds from incompressible flow to hypersonic velocities.[22-25] In laminar flow $\alpha_{SV} \approx 1.0\ \theta_c$, whereas the turbulent value is $\alpha_{SV} = 1.3\ \theta_c$. Asymmetric vortex shedding starts when the angle of attack exceeds the total included cone angle,[6,8] i.e., $\alpha_{AV} = 2\ \theta_C$. As long as the nose is slender, $\theta_N < 15$ deg, adding a cylindrical afterbody does not decrease α_{AV} significantly. However, for nonslender nose tips, $\theta_N > 25$ deg, α_{AV} is determined mainly by the body l/d. Fiechter[26] observed asymmetric vortex shedding starting at station x when $\alpha = 4.2\ d/x$. This value of α_{AV} agrees well with the experimental results in Refs. 6 and 8 for large l/d. Unsteady vortex shedding has been observed to occur at $\alpha \geq 60$ deg in several independent tests.[1,8,26] In addition to this expected unsteadiness when α approaches 90 deg there is also an unsteady phenomenon at incipient asymmetric vortex shedding, i.e., when $\alpha \approx \alpha_{AV}$. Lamont and Hunt[18] have observed this on-off asymmetric vortex shedding. It is conceivable that an aircraft or missile maneuver could "lock in" this asymmetry, thus effectively extending the α range of asymmetric vortex shedding.

In the high-angle-of-attack range ($\alpha_{AV} \leq \alpha < \alpha_{UV}$), the axial flow component is just strong enough to organize the leeside wake into vortex pairs. The circumferential location of the separation point (the vortex shedding point) and the vortex strength are determined almost entirely by the crossflow component. Thus, the circumferential separation locations on a slender body in this angle-of-attack range are strongly related to those for a cylinder normal to the flow. Atraghji's data[13] show that the separation locations on a slender body at angle of attack are bounded by the two-dimensional cylinder separation points (Fig. 6). (Displaced $\Delta\phi_S \approx 15$ deg because of the separation delay caused by three-dimensional flow effects.) The oilflow photographs show how the trajectory of the streamlines feeding the leeside vortices is elevated above the freestream flow through an angle (σ-α) due to the acceleration of the crossflow component around the body (Fig.

7). Clark and Peoples also present flow visualizations results showing this streamline elevation.[9] The condition of the boundary layer at separation is determined by the flow following this path. Aside from the initial "transient," the streamline is contained in the intersection between the cylinder and a plane at angle σ relative to the axis. The major concern is with defining the critical Reynolds number (where the side force is maximum). Thus, we shall use the arc length between the stagnation point and the lateral meridian as the characteristic length for the effective Reynolds number. Relating this to the two-dimensional reference flow defines the following effective diameter in the A-A plane (see Fig. 7):

$$d^*/d = (1/\sqrt{2})\sqrt{1+\operatorname{cosec}^2\sigma} \tag{1}$$

The corresponding Reynolds number ratio is

$$(Re)_{\text{eff}}/Re_d = (d^*/d)\cos(\sigma-\alpha) \tag{2}$$

With $\sigma = \tan^{-1}(2\tan\alpha)$ for the potential flow over a cylinder, the effective Reynolds number becomes

$$\frac{(Re)_{\text{eff}}}{Re_d} = \frac{\sqrt{1+8\tan^2\alpha}}{\sqrt{8}\tan\alpha}\left[\frac{(1+2\tan^2\alpha)}{\sqrt{(1+\tan^2\alpha)(1+4\tan^2\alpha)}}\right] \tag{3}$$

An earlier version of Eq. (3), in which $\sigma = 2\alpha$ was assumed,[27] has been shown by Clark[28] to be superior to other suggested formulations in correlating cross-flow drag measurements for slender missile configurations in the α range of symmetric and asymmetric vortex shedding ($20 \le \alpha \le 60$ deg). Applying the more accurate definition of $(Re)_{\text{eff}}$ given by Eq. (3) significantly improves the correlation for the low α range ($20 \le \alpha \le 30$ deg). For the α range where asymmetric vortex shedding occurs ($30 \le \alpha \le 60$ deg), approximating Eq. (3) by $(Re)_{\text{eff}} = Re_d$ causes less than 10% error, which usually is well within the experimental data scatter.

At the lower angles of attack, the boundary-layer transition is likely to occur through crossflow-induced vorticity effects,[29-32] and Eq. (3) will not be applicable. Thus, for all practical purposes,

$$(Re)_{\text{eff}} \approx Re_d \tag{4}$$

For the case that the body diameter is not constant, e.g., for the pointed noses of missiles and aircraft, an equivalent cylinder diameter (d_{eq}) is used, where d_{eq} is the arithmetic mean of the diameter at the stagnation point and the diameter at the aerodynamic center ($\bar{d}$). For a cone, one obtains

$$d_{eq} = \frac{\bar{d}}{2}\left[\frac{4\tan\alpha+\tan\theta_c}{2\tan\alpha+\tan\theta_c}\right] \tag{5}$$

where $\bar{d} = 2d_B/3$ for a sharp cone.

The maximum vortex-induced side force on a slender body in the critical angle-of-attack range will occur when the effective Reynolds number is transitional, and it is possible to have supercritical separation on one side of the body and subcritical separation on the other. This explains why the effective crossflow Reynolds number for the maximum side force measured by Nelson and Fleeman[7] correlates with the critical Reynolds number for a cylinder normal to the flow (Fig. 8).[33] The maximum stationary vortex asymmetry that

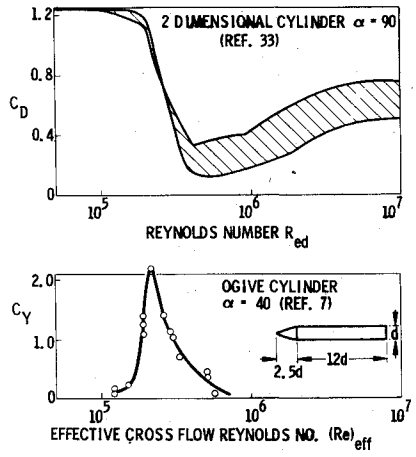

Fig. 8 Comparison of critical Reynolds number effects.

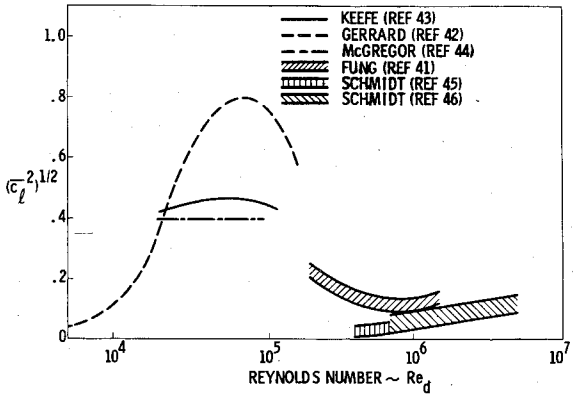

Fig. 9 Root-mean-square fluctuating lift measurements for two-dimensional cylinders normal to the flow.

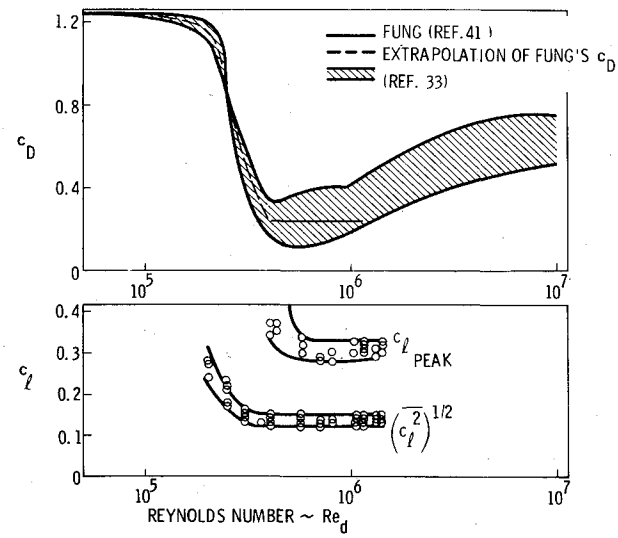

Fig. 10 Comparison of root-mean-square and peak lift coefficients with cylinder drag curve for a cylinder normal to the flow.

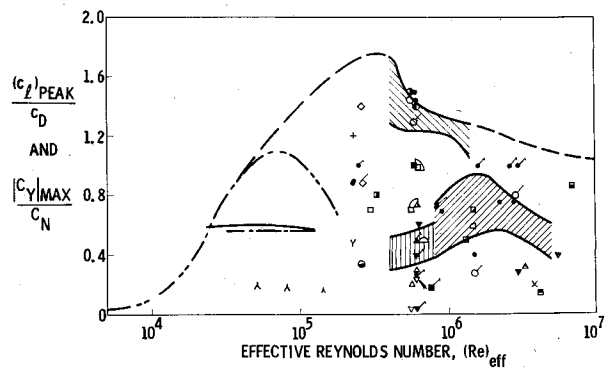

Fig. 11 Comparison of peak lift/drag ratio on cylinders normal to the flow with peak side-force/normal-force ratio.

can be realized for a slender body at a given average effective crossflow Reynolds number $(Re)_{eff}$ is bounded by the maximum unsteady asymmetry that occurs on a cylinder normal to the flow at the same Reynolds number based on the diameter Re_d. That the static data are bounded by the instantaneous peak of the dynamic data when flow separation and associated vortex shedding are involved is illustrated by many examples from the literature, e.g., the dynamic overshoot of drag for impulsively started cylinders and plates,[34] the delay of separation on rotating cylinders,[35] the delay of airfoil stall and the resulting overshoot of the static lift maximum due to pitch oscillations,[36-38] sudden aircraft pull-up maneuvers,[39] or leading-edge rotation.[40] Thus the peak unsteady lift coefficient on the two-dimensional cylinder

Table 1 Test conditions for data of Figs. 11 and 14

2-D CYLINDER				
SYMBOL	REF	M	FORCE RATIO	
	46	0.4	$\lvert c_\ell \rvert_{PEAK}/c_D$ & $\lvert \Delta c_D \rvert_{PEAK}/c_D$	
	43			
	42			
	44			
	45			
	41			
	INTERPOLATION AND EXTRAPOLATION			

3-D DATA					
SYMBOL	REF	M	CONFIG	ℓ/d	FORCE RATIO
	8	0.25	OGIVE	3.5	$\lvert C_Y \rvert_{MAX}/C_N$
	10	0.25		3.5	$\lvert C_Y \rvert_{MAX}/C_N$
		0.6			
		0.8			
		0.9			
	4	LOW SUBSONIC			$\lvert C_Y \rvert_{MAX}/C_N$ & $\Delta C_N/C_N$
	4	LOW SUBSONIC			$\lvert C_Y \rvert_{MAX}/C_N$
	20	0.25			
		0.4			
		0.6			
		0.7			
	10	0.25		5.0	
		0.6			
		0.8			
		0.9			
	20	0.25	OGIVE-CYL	7.0	
		0.42			
		0.62			
		0.72			
	4	0.25	CONE	16°	$\lvert C_Y \rvert_{MAX}/C_N$ & $\Delta C_N/C_N$
	4	LOW SUBSONIC	PARABOLID	3.5	$\lvert C_Y \rvert_{MAX}/C_N$
	14	0.57	OGIVE-CYL	8.18	
	15	0.6		15	
	15			11	
	13	0.5		17	
			CONE-CYL.	17	
	10	0.25	CONE-CYL.	11	
		0.6	CONE	20°	$\lvert C_Y \rvert_{MAX}/C_N$
		0.8			
	20	0.25	OGIVE-CYL. DETACHED	3.5(?)	$\lvert C_Y \rvert_{MAX}/C_N$ & $\Delta C_N/C_N$
Y	7	0.6	OGIVE-CYL.	14.5	$\lvert C_Y \rvert_{MAX}/C_N$
λ	21	LOW SUBSONIC	" "	15.0	$\lvert C_Y \rvert_{MAX}/C_N$

($c_{l_{peak}}$) represents the upper bound for the maximum steady side-force coefficient for the three-dimensional case ($\lvert C_Y \rvert_{max}$). This implicitly assumes that the axial flow component organizes even the random wake that occurs at supercritical Reynolds number into pairs of vortices, as indicated in Fig. 6.[13] The normalizing in-plane force coefficients are the steady cylinder drag coefficient c_D and the normal force coefficient C_N, respectively. Thus,

$$\frac{d}{dx}\left(\frac{\lvert C_Y \rvert_{max}}{C_N}\right) = \left[\frac{c_{l_{peak}}}{(\bar{c}_l^{\,2})^{1/2}}\right]\left[\frac{(\bar{c}_l^{\,2})^{1/2}}{c_D}\right] = \frac{c_{l_{peak}}}{c_D} \qquad (6)$$

This peak unsteady lift/drag ratio for the two-dimensional case provides the upper bound for the steady, three-dimensional side-force/normal-force ratio.

Root-mean-square (rms) lift measurements from a number of sources[41-46] are summarized in Fig. 9 for cylinders normal to the flow. For subcritical Reynolds numbers ($Re_d \leq 0.2\times10^6$), the unsteady lift varies harmonically, and $c_{l_{peak}}/(\bar{c}_l^{\,2})^{1/2} = \sqrt{2}$. For the random wake, the measured ratio $c_{l_{peak}}/(\bar{c}_l^{\,2})^{1/2}$ varies from 2.7 at $Re_d = 0.4\times10^6$ to 2.2 at $Re_d = 1.4\times10^6$, as indicated by Fung's data (Fig. 10).[41] It should be noted that Fung's results[41] differ significantly from Schmidt's.[45,46] Schmidt suggests that these differences are the result of roughness effects; thus, his smoother model shows lower rms lift values.[45,46] We are interested in defining the greatest vortex asymmetry possible in order to bound the maximum side force. (The rough data may, of course, also be more representative for flight hardware.) Therefore, Fung's results best suit our purposes.

The two-dimensional peak lift/drag ratio $c_{l_{peak}}/c_D$ from the unsteady cylinder data successfully bounds the three-dimensional side-force/normal-force ratio $\lvert C_Y \rvert_{max}/C_N$ (Fig. 11). (See Table 1 for detailed information about the experimental results.) Fung's $c_{l_{peak}}/(\bar{c}_l^{\,2})^{1/2}$ ratio from Fig. 10 is applied to both Fung's and Schmidt's results. The interpolation through the critical Reynolds number range ($0.2\times10^6 \leq Re_d \leq 0.4\times10^6$) was accomplished by assuming that $c_{l_{peak}}/(\bar{c}_l^{\,2})^{1/2}$ remained constant at the $Re_d = 0.4\times10^6$ level of 2.7. The mean value of c_D indicated in Fig. 10 was used through the critical Reynolds number range. It can be seen that the data for noses fall near the limiting boundary,

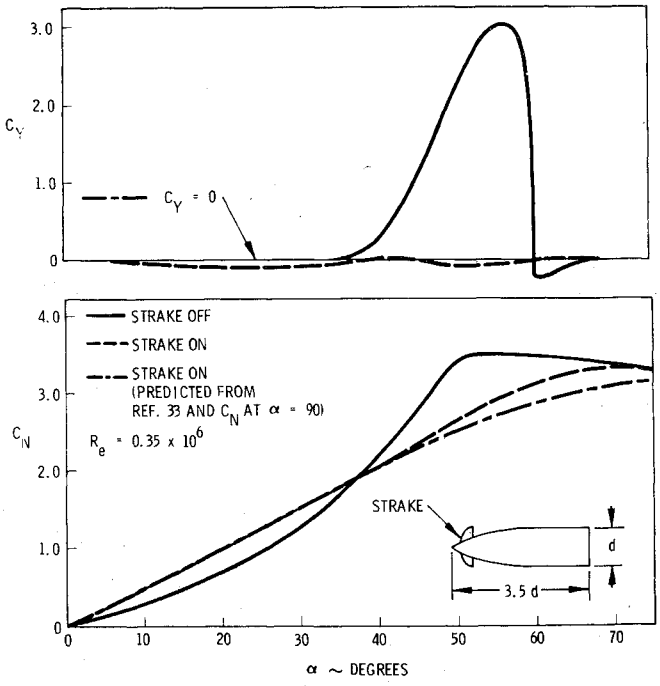

Fig. 12 Comparison of symmetric and asymmetric vortex shedding.[4]

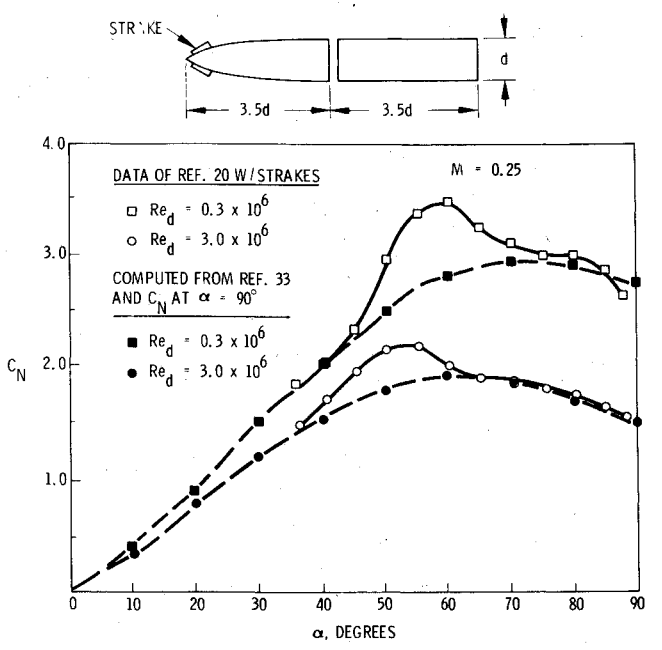

Fig. 13 Comparison of measured and predicted normal-force coefficient for symmetric vortices.

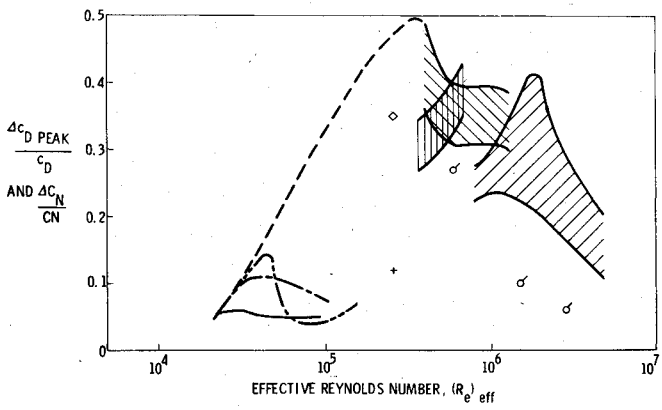

Fig. 14 Comparison of peak drag ratio on a cylinder normal to the flow with the peak normal-force ratio.

whereas the data for nose-cylinders tend to have lesser side-force ratios as their multiple vortex pairs produce opposing side-force contributions (Fig. 11).

Maximum Additional Normal Force

Figure 1 shows that the normal force peaks at the same angle of attack as does the side force. One would expect that, when the vortices become asymmetric, the normal force will also increase, and this increase will correspond to the unsteady in-plane (drag) force on a two-dimensional cylinder. Thus, the corollary to Eq. (6) is

$$\frac{d}{dx}\left(\frac{\Delta C_N}{C_N}\right)=\left[\frac{\Delta c_{D\text{peak}}}{(\overline{\Delta c_D}^2)^{1/2}}\right]\left[\frac{(\overline{\Delta c_D}^2)^{1/2}}{c_D}\right]=\frac{\Delta c_{D\text{peak}}}{c_D} \quad (7)$$

where ΔC_N is the additional vortex-induced normal force. It is presumed that

$$\Delta c_{D\text{peak}}/(\Delta \bar{c}_D{}^2)^{1/2}=c_{L\text{peak}}/(\bar{c}_l{}^2)^{1/2} \quad (8)$$

The data of Coe et al.[4] show that, when strakes were added to an ogive to eliminate the vortex asymmetry, both the side force and the additional normal force were eliminated simultaneously (Fig. 12).[4] Using Jorgensen's[33] extension of the Allen and Perkins[47] crossflow drag techniques, the normal-force coefficient curves for symmetric vortex shedding were computed. (The effective crossflow drag coefficient was obtained from C_N at $\alpha=90$ deg.) The computed normal-force curve underpredicts the normal-force data in the region where the vortex-induced loads are a maximum (Fig. 12). A more severe underprediction is obtained when Jorgensen's technique is compared to the data of Ref. 20 (Fig. 13) for a 3.5 *l/d* ogive in the presence of a 3.5 *l/d* cylindrical afterbody. (The afterbody loads were not measured.) Evidently this reflects a deficiency of the theory in predicting the symmetric vortex-induced loads. For this reason, the additional normal force (ΔC_N) has been computed only for cases where data were available with and without strakes. This limited sample is bounded by the $\Delta c_{D\text{peak}}/(\bar{c}_D{}^2)^{1/2}$ limits determined from the two-dimensional cylinder data, as demonstrated in Fig. 14. (See Table 1 for information about experimental data.)

Conclusions

A method for predicting the maximum possible vortex-induced side force at high angle of attack and zero sideslip has been presented. The method uses the peak unsteady lift-to-drag ratio on a two-dimensional cylinder normal to the flow to bound the steady side-force to normal-force ratio. An effective Reynolds number is defined for the three-dimensional flow and used to relate Reynolds number effects. Similarly, the additional lift induced by asymmetric vortices at high angle of attack is bounded by the unsteady peak drag to steady drag ratio for a two-dimensional cylinder normal to the flow. This technique should be useful for specifying the maximum possible side force for control system design of missiles and aircraft.

References

[1] Thomson, K. D. and Morrison, D. F., "The Spacing, Position and Strength of Vortices in the Wake of Slender Cylindrical Bodies at Large Incidence," *Journal of Fluid Mechanics*, Vol. 50, Pt. 4, Dec. 1971, pp. 751-783.

[2] Fidler, J. E. and Bateman, M. C., "Asymmetric Vortex Effects on Missile Configurations," *Journal of Spacecraft and Rockets*, Vol. 12, Nov. 1975, pp. 674-681.

[3] Chambers, J. P., Anglin, E. L., and Bowman, J. B. Jr., "Effects of Pointed Nose on Spin Characteristics of a Fighter Airplane Model Including Correlation with Theoretical Calculations," NASA TN D-5921, 1970.

[4] Coe, P. L. Jr., Chambers, J. R., and Letko, W., "Asymmetric Lateral-Directional Characteristics of Pointed Bodies of Revolution at High Angles of Attack," NASA TN D-7095, Nov. 1972.

[5] Pick, G. S., "Investigation of Side Forces on Ogive-Cylinder Bodies at High Angles of Attack in the $M=0.5$ to 1.1 Range," AIAA Paper 71-750, AIAA 4th Fluid and Plasma Dynamics Conference, Palo Alto, Calif., June 21-23, 1971.

[6] Keener, E. R. and Chapman, G. T., "Onset of Aerodynamic Side Forces at Zero Sideslip of Symmetric Bodies at High Angles of Attack," AIAA Paper 74-770, Anaheim, Calif., Aug. 5-9, 1974.

[7] Nelson, R. C. and Fleeman, E. L., "High Angle-of-Attack Aerodynamics on a Slender Body with a Jet Plume," *Journal of Spacecraft and Rockets*, Vol. 12, Jan. 1975, pp. 12-16.

[8] Keener, E. R., Chapman, G. T., and Druse, R. L., "Effects of Mach Number and Afterbody Length on Onset of Asymmetric Forces on Bodies at Zero Sideslip and High Angles of Attack," AIAA Paper 76-66, AIAA 14th Aerospace Sciences Meeting, Washington, D. C., Jan. 26-28, 1976.

[9] Clark, W. H. and Peoples, J. R., "Occurrence and Inhibition of Large Yawing Moments During High-Incidence Flight of Slender Missile Configurations," *Journal of Spacecraft and Rockets*, Vol. 10, Aug. 1973, pp. 510-519.

[10] Keener, E. R. and Taleghani, J., "Wind Tunnel Investigation of the Aerodynamic Characteristics of Five Forebody Models at High Angles of Attack at Mach Numbers from 0.25 to 2," NASA TM X-73,076, Dec. 1975.

[11] Chapman, G. T., Keener, E. R., and Malcolm, G., "Asymmetric Aerodynamic Forces on Aircraft Forebodies at High Angles of Attack – Some Design Guides," *AGARD Flight Mechanics Panel Specialists Meeting: Stall/Spin Problem of Military Aircraft*, NASA Ames Research Center, Moffet Field, Calif., Paper 16, Nov. 18-21, 1976.

[12] Wardlaw, A. B. Jr. and Morrison, A. M., "Induced Side Forces at High Angle of Attack," *Journal of Spacecraft and Rockets*, Vol. 13, Oct. 1976, pp. 589-593.

[13] Atraghji, E. G., "The Influence of Mach Number Reynolds Number, Semi-nose Angle and Roll Rate on the Development of the Forces and Moments Over a Series of Long Slender Bodies of Revolution at Incidence," National Research Council, Ottawa, Canada, NAE High Speed Aerodynamic Section Rept. 5×5/0020, Sept. 6, 1967.

[14] Brown, R. G., "On the Asymmetrical Aerodynamic Forces of Slender Bodies of Revolution," private communication, 1966.

[15] Kubin, J. S., "An Analysis of Steady Asymmetric Vortex Shedding From a Missile at High Angles of Attack," Air Force Inst. of Technology, AD-774 390, Nov. 1973.

[16] Smith, L. H. and Nunn, R. H., "Aerodynamic Characteristics of an Axisymmetric Body Undergoing a Uniform Pitching Motion," *Journal of Spacecraft and Rockets*, Vol. 13, Jan. 1976, pp. 8-14.

[17] Hassel, L. J. Jr. and Hewes, D. E., "Investigation of the Subsonic Stability and Control Characteristics of a 1/7 Scale Model of the North Americal X-15 Airplane with and without Fuselage Forebody Strakes," NASA TM X-210, Feb. 1960.

[18] Lamont, P. J. and Hunt, B. L., "Pressure and Force Distributions on a Sharp Nosed Circular Cylinder at Large Angles of Inclination to a Uniform Subsonic Stream," *Journal of Fluid Mechanics*, Vol. 76, Pt. 3, Aug. 1976, pp. 519-559.

[19] Lamont, P. J. and Hunt, B. L., "Prediction of Aerodynamic Out-of-Plane Forces on Ogive-Nosed Circular Cylinders," *Journal of Spacecraft and Rockets*, Vol. 14, Jan. 1977, pp. 38-44.

[20] Keener, E. P., Chapman, G. T., Cohen, L., and Taleghani, J., "Side Forces on a Tangent Ogive Forebody with a Fineness Ratio of 3.5 at High Angles of Attack and Mach Numbers From 0.1 to 0.7," NASA TMX-3437, Feb. 1977.

[21] Smith, L. H., "Aerodynamic Characteristics of an Axisymmetric Body Undergoing a Uniform Pitching Motion," Ph.D. Thesis, Naval Postgraduate School, Monterey, Calif., Dec. 1974.

[22] Rainbird, W. J., "Turbulent Boundary-Layer Growth and Separation on a Yawed Cone," *AIAA Journal*, Vol. 6, Dec. 1968, pp. 2410-2416.

[23] Rainbird, W. J., Crabbe, R. S. and Jurewicz, L. S., "A Water Tunnel Investigation of the Flow Separation About Circular Cones at Incidence," National Research Council, National Aeronautical Establishment, Ottawa, Canada, Aero Rept. LR-385, Sept. 1963.

[24] Tracy, R. R., "Hypersonic Flow Over a Yawed Circular Cone," California Inst. of Technology, Pasadena, Calif., CIT/GAL Memo. 69, Aug. 1963.

[25] Stetson, K. J. and Ojdana, E. S., "Hypersonic Laminar Boundary Layer Separation on a Slender Cone at Angle of Attack," *AIAA Journal*, Vol. 10, May 1972, pp. 642-648.

[26] Fiechter, M., "Über Wirbelsysteme an schlanken Rotationskörpern und ihren Einfluss auf die aerodynamischen Beiwerte," Franco-German Research Inst., Saint-Louis, Rapport-Bericht 10/66, Dec. 1966.

[27] Reding, J. P. and Ericsson, L. E., "Maximum Vortex-Induced Side Forces on Slender Bodies," *High Angle of Attack Aerodynamic Working Group Meeting*, Redstone Arsenal, Ala., March 16-17, 1977.

[28] Clark, W. H., "Body Vortex Formation on Missiles in Incompressible Flows," AIAA Paper 77-1154, AIAA 1977 Atmospheric Flight Mechanics Conference, Hollywood, Fla., Aug. 1977.

[29] Owen, P. R. and Randall, D. G., "Boundary Layer Transition on a Swept-Back Wing," Royal Aircraft Establishment, Memo. Aero 277, June 1952.

[30] Chapman, G. T., "Some Effects of Leading-Edge Sweep on Boundary Layer Transition at Supersonic Speeds," NASA TN D-1075, Sept. 1961.

[31] Pate, S. R. and Adams, J. C., "Hypersonic Simulation for Lifting Body Transition Studies," *Proceedings of the Boundary Layer Transition Workshop*, Paper 6, Vol. III, Aerospace Corp., Rept. TOR-0172 (S2816-16)-5, Nov. 1971.

[32] Pate, S. R., "Experimental and Analytical Investigation of Boundary-Layer Transition on Swept Wings at Mach Numbers 2.5 to 5," Arnold Engineering Development Center, AEDC-TR-67-186, Oct. 1967.

[33] Jorgensen, L. H., "Prediction of Static Aerodynamic Characteristics for Space-Shuttle-Like and Other Bodies at Angles of Attack from 0° to 180°," NASA TN D-6996, June 1973.

[34] Sarpkaya, T., "Separated Flow About Lifting Bodies and Impulsive Flow About Cylinders," *AIAA Journal*, Vol. 4, March 1966, pp. 414-420.

[35] Moore, F. K., "On The Separation of Unsteady Laminar Boundary Layer," *IUTAM Symposium on Boundary Layer Research*, Freiburg, Aug. 26-29, 1957, pp. 296-311.

[36] Ericsson, L. E. and Reding, J. P., "Dynamic Stall Analysis in Light of Recent Numerical and Experimental Results," *Journal of Aircraft*, Vol. 13, April 1976, pp. 248-255.

[37] Ericsson, L. E. and Reding, J. P., "Spilled Leading Edge Vortex Effects on Dynamic Stall Characteristics," *Journal of Aircraft*, Vol. 13, April 1976, pp. 313-315.

[38] Ericsson, L. E. and Reding, J. P., "Further Consideration of Spilled Leading Edge Vortex Effects on Dynamic Stall," *Journal of Aircraft*, Vol. 14, June 1977, pp. 601-603.

[39] Spreiter, J. P., Galster, G. M., and Blair, W. K., "Effect of Mach and Reynolds Number on the Maximum Lift Coefficient Obtainable in Gradual and Abrupt Stalls of a Pursuit Airplane Equipped with a Low Drag Wing," NACA RM A5G06, 1945.

[40] Johnson, W. S., Tennant, J. S., and Stamps, R. E., "Leading-Edge Rotating Cylinder for Boundary-Layer Control on Lifting Surfaces," *Journal of Hydronautics*, Vol. 9, April 1975, pp. 76-78.

[41] Fung, Y. C., "Fluctuating Lift and Drag Acting on a Cylinder in a Flow at Supercritical Reynolds Numbers," *Journal of the Aerospace Sciences*, Vol. 27, Nov. 1960, pp. 801-814.

[42] Gerrard, J. H., "An Experimental Investigation of the Oscillating Lift and Drag of a Circular Cylinder Shedding Turbulent Vortices," *Journal of Fluid Mechanics*, Vol. 11, Pt. 2, Sept. 1961, pp. 244-256.

[43] Keefe, R. T., "An Investigation of the Fluctuating Forces Acting on a Stationary Circular Cylinder in a Subsonic Stream and of the Associated Sound Field," Univ. of Toronto, UTIA Rept. 76, 1961.

[44] McGregor, D. M., "An Experimental Investigation of the Oscillating Pressure on a Circular Cylinder in a Fluid Stream," Univ. of Toronto, Tech Note 14, 1957.

[45] Schmidt, L. V., "Measurements of Fluctuating Air Loads on a Cylinder," *Journal of Aircraft*, Vol. 2, Jan.-Feb. 1965, pp. 49-55.

[46] Schmidt, L. V., "Fluctuating Force Measurements upon a Circular Cylinder at Reynolds Numbers Up to 5×10^6," *Meeting on Ground Wind Load Problems in Relation to Launch Vehicles*, NASA Langley Research Center, Paper 19, June 7-8, 1966.

[47] Allen, J. H. and Perkins, E. W., "A Study of Effects of Viscosity On Flow Over Slender Inclined Bodies of Revolution," NACA Rept. 1048, 1951.